

Multivariable Painlevé-II equation: connection formulas for asymptotic solutions

Nikolai A. Sinitsyn^{1,*}

¹Theoretical Division, Los Alamos National Laboratory, Los Alamos, New Mexico 87545, USA

(Dated: October 2025)

It is shown that a generalization of the Painlevé-II equation (P-II) to a system of coupled equations with symmetry breaking terms is integrable. A Lax pair for this system is used to relate the asymptotic behavior of the solutions at different infinities via an asymptotically exact WKB approach. The analysis relies on an exact solution of the quantum mechanical Demkov-Osherov model (DOM). An application to the problem of unstable vacuum decay during a second order phase transition provides precise scaling of the number of excitations, including subdominant contributions.

I. INTRODUCTION

Theoretical physics relies on a set of special functions, which are usually solutions of differential equations whose properties can be understood in great detail. Thus, throughout the 20th century, a physicist's standard toolbox included knowledge of solvable linear ordinary second order differential equations. The commonly used property of such equations is the existence of *connection formulas* that relate the parameters of the asymptotic solutions in different limits.

Towards the end of the 20th century, the connection formulas for asymptotic solutions of certain second order *nonlinear* differential equations were also derived. For example, the homogeneous P-II

$$u''(x) = xu(x) - 2u(x)^3, \quad (1)$$

is one of the most frequently encountered nonlinear second order differential equations in theoretical physics. Connection formulas [1, 2] relate the behavior of $u(x)$ in the $x \rightarrow \pm\infty$ limits. They were used to write integrals of Painlevé transcendents over x in terms of classical special functions [3–5]. Applications of such connection formulas have already been numerous, including in ultracold atoms [6, 7], viscous flow [8], spectroscopy [9], quantum phase transitions [10], quantum information [11], plasma physics [12, 13], liquid crystals [14], and stochastic processes [15].

In a seemingly different direction, there is a progress on solvable *higher-order linear* systems, including the multistate Landau-Zener models [16–19] and solvable quantum quench models [20–26], which describe interacting quantum systems of potentially combinatorial complexity under explicitly time-dependent conditions. This raises the question of whether there exist practically interesting higher-order *systems* of nonlinear differential equations that are integrable and possess simple connection formulas for the asymptotic behavior of their solutions as well.

The present Letter provides exact analytical connection formulas for a multivariable generalization of P-II. This nonlinear system is shown to be related to the Demkov-Osherov

model (DOM) [10, 27], which is one of the earliest known solvable generalizations of the quantum mechanical Landau-Zener model to an arbitrary number of interacting states with linearly time-dependent parameters. As the class of solvable multistate Landau-Zener systems is known to be large [28, 29], its relevance to solvability of nonlinear systems suggests that the class of integrable multi-variable generalizations of the Painlevé equations with tractable asymptotic behavior may be as large. Thus, the synergy between the two research directions in mathematical physics may enable analytical treatment of more complex nonlinear problems.

II. DEFINITION OF THE MODEL

Let a system of n coupled nonlinear differential equations depend on n parameters $e_1 < e_2 < \dots < e_n$:

$$\begin{aligned} u_1''(x) &= xu_1(x) - 2u_1(x) \sum_{k=1}^n u_k^2(x) + e_1 u_1(x), \\ u_2''(x) &= xu_2(x) - 2u_2(x) \sum_{k=1}^n u_k^2(x) + e_2 u_2(x), \\ &\dots \\ u_n''(x) &= xu_n(x) - 2u_n(x) \sum_{k=1}^n u_k^2(x) + e_n u_n(x). \end{aligned} \quad (2)$$

A shift, $x \rightarrow x - e_1$, sets $e_1 = 0$, which will be assumed here.

The system in Eq. (2) is integrable. The asymptotic behavior of the solution as $x \rightarrow \pm\infty$ can be connected by analytic formulas. The *first observation* that enables this result is that the system in Eq. (2) is obtained as a consistency condition

$$\left(\frac{\partial H}{\partial x} - \frac{\partial H_1}{\partial t} \right) - i[H, H_1] = 0, \quad (3)$$

for two $(n+1)$ -dimensional Hermitian matrices, $H(t, x)$ and $H_1(t, x)$, given explicitly by

$$H = A - 4tB + 2C, \quad H_1 = \begin{bmatrix} t & -u_1 & \cdots & -u_{n-1} & -u_n \\ -u_1 & -t & 0 & \cdots & 0 \\ \vdots & \vdots & \ddots & \vdots & \vdots \\ -u_{n-1} & 0 & \cdots & -t & 0 \\ -u_n & 0 & \cdots & 0 & -t \end{bmatrix}, \quad (4)$$

where

$$A = \begin{bmatrix} 4t^2 + x - 2 \sum_{k=1}^n u_k^2(x) & 0 & \cdots & \cdots & 0 \\ 0 & -(4t^2 + x + 2e_1) + 2u_1^2 & 2u_1u_2 & \cdots & 2u_1u_n \\ \vdots & 2u_2u_1 & -(4t^2 + x + 2e_2) + 2u_2^2 & \ddots & 2u_2u_n \\ \vdots & \vdots & \ddots & \ddots & \vdots \\ 0 & 2u_nu_1(x) & 2u_nu_2 & \cdots & -(4t^2 + x + 2e_n) + 2u_n^2 \end{bmatrix},$$

$$B = \begin{bmatrix} 0 & u_1 & \cdots & u_n \\ u_1 & 0 & \cdots & 0 \\ \vdots & \vdots & \ddots & \vdots \\ u_n & 0 & \cdots & 0 \end{bmatrix}, \quad C = \begin{bmatrix} 0 & -iu_1' & \cdots & -iu_3'(x) \\ iu_1' & 0 & \cdots & 0 \\ \vdots & \vdots & \ddots & \vdots \\ iu_n' & 0 & \cdots & 0 \end{bmatrix}, \quad \text{where } u_k \equiv u_k(x), \quad u_k' \equiv \frac{du_k(x)}{dx}. \quad (5)$$

Thus, if the functions $u_k(x)$, $k = 1, \dots, n$, satisfy Eq. (2), then the Hamiltonians H and H_1 from Eq. (4) satisfy the consistency condition (3). Similar properties have been previously used in studies of the Painlevé [2] and many other nonlinear differential equations of mathematical physics [30]. Therefore, the fact that similar pairs of Hamiltonians can be found for higher-order nonlinear equations is not surprising. However, the consistency conditions do not guarantee that the WKB analysis that they enable leads to analytically tractable equations. The *second observation* that enables the following results is that such a WKB analysis for the system in Eq. (2) can be performed completely analytically.

III. THE SYSTEM OF TWO VARIABLES: MAIN RESULTS

Derivation of the connection formulas for the entire system in Eq. (2) is somewhat involved. The goal of this brief Letter is, instead, to announce their existence and demonstrate the consequences of the integrability for the simplest nontrivial case of only two variables, $n = 2$ in Eq. (2), while leaving many details to future publications. For $n = 2$, the system in Eq. (2) reduces to

$$u_1''(x) = xu_1(x) - 2u_1(x) [u_1^2(x) + u_2^2(x)], \quad (6)$$

$$u_2''(x) = xu_2(x) - 2u_2(x) [u_1^2(x) + u_2^2(x)] - eu_2(x), \quad (7)$$

where $e > 0$.

A. Connection formulas

Standard perturbative analysis [31] fixes the asymptotic behavior of the solution for the system in Eqs. (6) and (7) as $x \rightarrow -\infty$ up to four parameters, $\alpha_{1,2}$ and $\varphi_{1,2}$, where $\alpha_{1,2} > 0$. Namely,

for $x \rightarrow -\infty$:

$$u_1 = \frac{\alpha_1}{(-x)^{1/4}} \sin \left[\frac{2}{3}(-x)^{3/2} + \frac{(3\alpha_1^2 + 2\alpha_2^2)}{4} \ln(-x) + \varphi_1 \right],$$

$$u_2 = \frac{\alpha_2}{(-x + e)^{1/4}} \sin \left[\frac{2}{3}(-x + e)^{3/2} + \frac{(3\alpha_2^2 + 2\alpha_1^2)}{4} \ln(-x) + \varphi_2 \right]. \quad (8)$$

The constant parameters $\alpha_{1,2}$ and $\varphi_{1,2}$ will be referred to as initial amplitudes and phases, respectively.

As $x \rightarrow +\infty$, the trivial perturbation theory easily fixes only the leading x -dependent terms in the oscillation phases, while the sub-leading terms, starting with the terms behaving as $\propto \ln x$, are derived using the WKB approach described in Section IV. The solution is finally, i.e., as $x \rightarrow +\infty$, parametrized by two positive amplitudes, ρ and A , two phases,

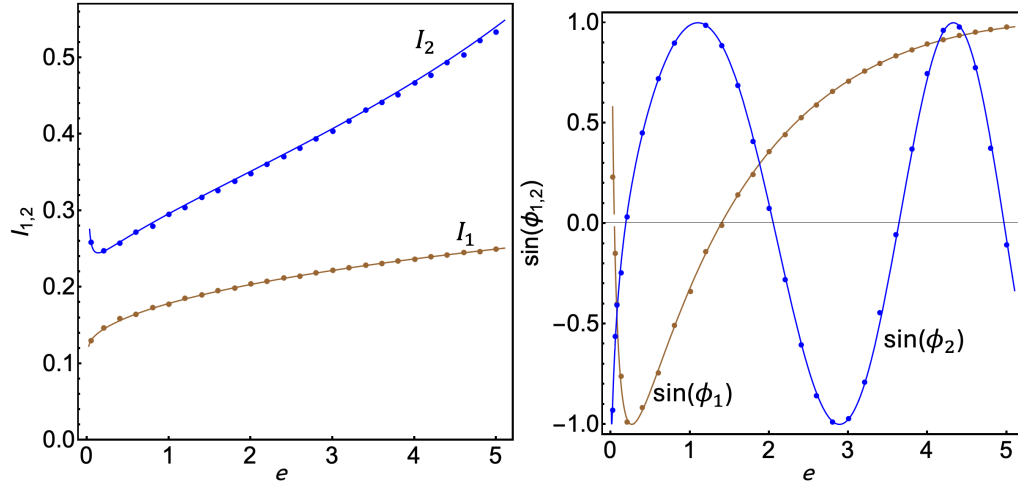


FIG. 1. Numerical test of Eqs. (14)-(17). Solid curves correspond to theoretical predictions for the dependence on the equation parameter $e \in (0.05, 5)$ (a) of the action variables I_1 (brown) and I_2 (blue); (b) of the angle-related variables $\sin \phi_1$ (brown) and $\sin \phi_2$ (blue). Discrete points correspond to results of numerical simulations. Both for analytical predictions and numerical calculations the initial conditions were chosen to be $\alpha_1 = 0.9, \alpha_2 = 0.8, \varphi_1 = \pi/2, \varphi_2 = \pi/3$. Simulations were performed in the interval $x \in (-5000, 5000)$ with a discretization step $dx = 0.00001$. The algorithm is described in [32]. Both theory and numerical simulations agree on that $\sigma = -1$ for all points here.

ϕ_1 and ϕ_2 , and one sign parameter, $\sigma = \pm 1$:

$$p_1 = e^{-\pi\alpha_1^2}, \quad p_2 \equiv e^{-\pi\alpha_2^2}, \quad (12)$$

For $x \rightarrow +\infty$:

$$u_1(x) = \sigma \sqrt{\frac{x}{2}} + \quad (9)$$

$$\sigma \frac{\rho}{(2x)^{1/4}} \cos \left[\frac{2\sqrt{2}}{3} x^{3/2} - \frac{3}{2} \rho^2 \ln x + \phi_1 \right],$$

$$u_2(x) = \sigma A \cos \left[\sqrt{e}x - \frac{A^2\sqrt{e}}{2} \ln x + \phi_2 \right]. \quad (10)$$

Let me define the following combinations of the final and initial parameters:

$$I_1 \equiv \frac{\rho^2}{2}, \quad I_2 \equiv \frac{A^2\sqrt{e}}{2}, \quad (11)$$

including two phases:

$$\Phi_1 \equiv \frac{\pi}{4} + \arg\Gamma \left(i \frac{\alpha_1^2}{2} \right) + \varphi_1 - \frac{3\alpha_1^2}{2} \ln 2 + \frac{\alpha_2^2}{2} \ln(e/4),$$

$$\Phi_2 \equiv \frac{\pi}{4} + \arg\Gamma \left(i \frac{\alpha_2^2}{2} \right) + \varphi_2 - \frac{3\alpha_2^2}{2} \ln 2 + \frac{\alpha_1^2}{2} \ln(e/4).$$

The *main result of this article* is the following connection formulas that relate the final parameters $\{\sigma, I_1, I_2, \phi_1, \phi_2\}$ to the set of initial parameters $\{p_1, p_2, \Phi_1, \Phi_2\}$ and the parameter of the equation, e :

$$\sigma = \text{sign}[\sin(\Phi_1)], \quad (13)$$

$$I_1 = -\frac{1}{4\pi} \ln \left(1 - p_1^2 p_2^2 \left| 1 + \frac{1-p_1}{p_1} e^{2i\Phi_1} + \frac{1-p_2}{p_1 p_2} e^{2i\Phi_2} \right|^2 \right), \quad (14)$$

$$\phi_1 = -\frac{3\pi}{4} - I_1 \cdot 7 \ln 2 + \arg\Gamma(2iI_1) - \arg \left(1 + \frac{1-p_1}{p_1} e^{2i\Phi_1} + \frac{1-p_2}{p_1 p_2} e^{2i\Phi_2} \right), \quad (15)$$

$$I_2 = -\frac{1}{\pi} \ln \left(2\sqrt{p_2 p_1 (1-p_1)} |\sin(\Phi_1)| \right) - 2I_1, \quad (16)$$

$$\phi_2 = \frac{3\pi}{4} - \frac{2}{3} e^{3/2} - I_2 \ln(4e^{1/2}) + \arg[\Gamma(iI_2)] - \arg(e^{i\Phi_2} + e^{-i\Phi_2} (p_1 + (1-p_1)e^{2i\Phi_1})). \quad (17)$$

B. Tests of connection formulas

The first test for the validity of Eqs. (13)-(17) is the observation that at $\alpha_2 = 0$, Eq. (7) has a trivial solution $u_2(x) = 0$,

which corresponds to $I_2 = 0$ and $u_1(x)$ satisfying Eq. (1). As expected, Eqs. (14) and (15) then reduce to the previously

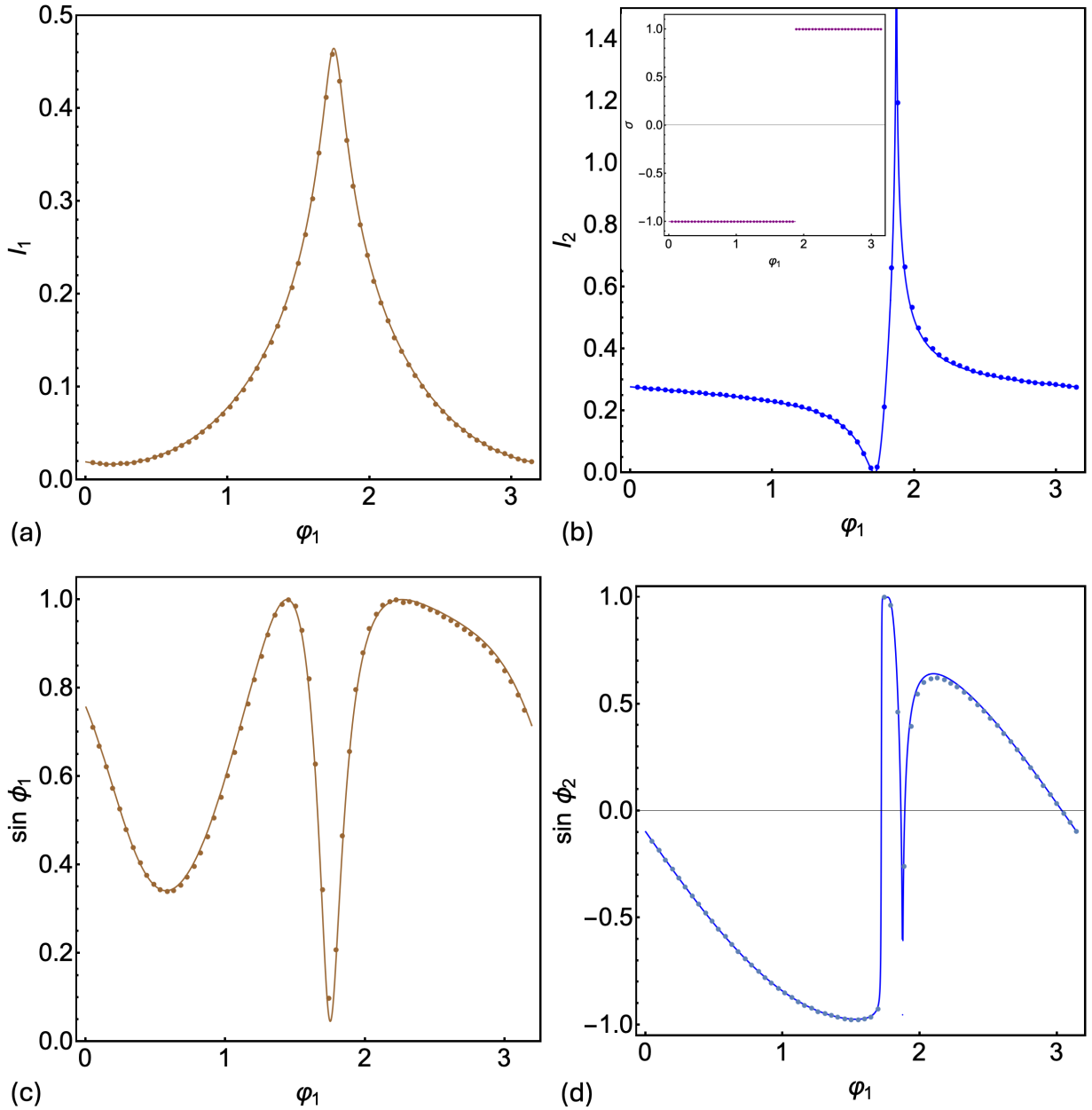


FIG. 2. Numerical test of Eqs. (13)-(17). Solid curves correspond to theoretical predictions for the dependence on the angle $\varphi_1 \in (0, \pi)$ (a,b) of the action variables I_1 (brown) and I_2 (blue), respectively; (c,d) of the angle-related variables $\sin \phi_1$ (brown) and $\sin \phi_2$ (blue), respectively. Discrete points correspond to results of numerical simulations. Both for analytical predictions and numerical calculations the initial conditions were chosen to be $e = 1$, $\alpha_1 = 0.8$, $\alpha_2 = 0.6$, $\varphi_2 = \pi/2$. Simulations were performed in the interval $x \in (-5000, 5000)$ with a discretization step $dx = 0.00001$. Inset in (b) shows the test of Eq. (13) for the sign σ dependence on φ_1 (purple).

known connection formulas for Eq. (1) listed in [2].

More generally, the connection formulas were tested numerically for x -evolution with Eqs. (6) and (7). Simulations were performed using the approach described in [32], which treats x as a time variable. The evolution was considered during $x \in (-5000, 5000)$ with initial parameters taken to be $O(1)$. After this interval, a small piece of the trajectory was recorded and the final parameters were inferred by the best fit of this piece with Eqs. (9) and (10).

The results are shown in Figs. 1 and 2. Since the angles $\phi_{1,2}$ are determined only up to an integer multiple of 2π , to obtain smooth curves, $\sin \phi_1$ and $\sin \phi_2$ are plotted instead of the angles themselves. Apparently, despite the highly non-linear and sometimes singular dependence of the final set of parameters on the initial ones, the numerical results appear to be in perfect agreement with the analytical predictions. Many other similar tests (not shown) were performed for different values, e.g., of $\alpha_{1,2}$, with the same conclusion.

Finally, let me comment on corrections to the connection formulas. For large but finite x , they appear starting with the terms $\propto 1/\sqrt{x}$, which decay relatively slowly. They can be calculated using the same WKB approach, but the complete study of such terms appears to be difficult due to the large number of diverse relevant contributions. Some of them are singular in the limit $e \rightarrow 0$. This is why the simulations were restricted to $e > 0.05$ – otherwise, a considerably larger integration interval is needed in order to achieve a comparable agreement with theoretical predictions.

Numerically, for the range of the tested parameters, with $e > 0.05$, there were two specific corrections observed that dominated over other terms of the same order in x . These two corrections can be easily included into the connection formulas, leading to noticeable accuracy improvements at large but finite x . First, the regular part of $u_1(x)$ in Eq. (9) is renormalized by interactions as

$$\sigma\sqrt{\frac{x}{2}} \rightarrow \sigma\sqrt{\frac{x - 2u_2(x)^2}{2}}, \quad (18)$$

where $u_2(x)$ is taken from Eq. (10). This correction vanishes as $\propto 1/\sqrt{x}$, but it is only a factor $\sim 1/x^{1/4}$ smaller than the leading oscillatory term in Eq. (9). Therefore, its effects are well visible during simulations as a slowly decaying modulation of oscillations in $u_1(x)$.

Second, there is a correction to ϕ_1 in Eq. (15) that follows from the renormalization of the energy of the state $|0\rangle$ in the WKB approach applied to the evolution along the path P_∞ (see Section IV for details). It can be included in the connection formulas by subtracting an additional term from the right hand side of Eq. (15):

$$\phi_1 \rightarrow \phi_1 - 2\pi I_2 \sqrt{\frac{e}{2x}}. \quad (19)$$

Although well suppressed, small effects of this correction were visible even for the longest simulations. This is attributed to its growth with e and the existence of singularities that make I_2 anomalously large at specific initial conditions.

IV. DERIVATION OF CONNECTION FORMULAS

A. Strategy

Consistency conditions (3) allow one to define a state vector, $|\Psi(t, x)\rangle$, as a solution of the two-time Schrödinger equation [30]

$$i\frac{d|\Psi\rangle}{dt} = H(t, x)|\Psi\rangle, \quad (20)$$

$$i\frac{d|\Psi\rangle}{dx} = H_1(t, x)|\Psi\rangle, \quad (21)$$

where H and H_1 are 3×3 matrices given by Eq. (4) for $n = 3$. The evolution operator U_P along an arbitrary path P in the

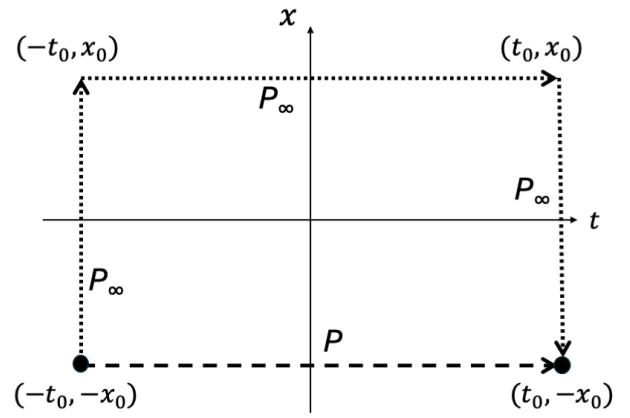


FIG. 3. An integration path P (dashed arrow) with $x_0 \rightarrow -\infty$ and $t \in (-t_0, t_0)$, where $t_0 \gg x_0$, is deformed into the path P_∞ , such that the horizontal segment of P_∞ lies at $x_0 \rightarrow +\infty$ and $t \in (-t_0, t_0)$ (dotted arrows). This deformation does not change the evolution operator in Eq. (22), since the initial and final points of the path remain unchanged. The vertical legs of P_∞ have $t = \pm t_0 \rightarrow \pm\infty$, which makes the evolution along them adiabatic.

two-time space (t, x) can be written as a path-ordered exponent:

$$U_P = \mathcal{T}_P e^{-i \int_P \{H dt + H_1 dx\}}, \quad (22)$$

where \mathcal{T}_P is the path ordering operator, such that factors corresponding to earlier points along P appear further to the right inside the product of evolution exponents $e^{-i \{H dt + H_1 dx\}}$.

Equation (22) can be written as

$$U_P = \mathcal{T}_P e^{\int_P \mathbf{A} \cdot d\boldsymbol{\tau}}, \quad (23)$$

where $\boldsymbol{\tau} \equiv (t, x)$ is the two-time point and $\mathbf{A} \equiv (-iH, -iH_1)$ is a non-Abelian field. This field is flat (has zero curvature) [18], so the result of the evolution in Eq. (23) depends only on the endpoints, which are $(-t_0, -x_0)$ and $(t_0, -x_0)$ in Fig. 3, but does not depend on the choice of the path connecting these points.

Thus, the evolution over the path P shown in Fig. 3 can be calculated in two ways. First, one can consider t changing in the interval $t \in (-t_0, t_0)$ at fixed negative $x = -x_0$. The evolution operator then takes the form

$$U_P = \mathcal{T}_t e^{-i \int_{-t_0}^{t_0} H(t, -x_0) dt}. \quad (24)$$

Alternatively, U_P can be obtained as an evolution operator along the path P_∞ in Fig. 3. The vertical legs of P_∞ correspond to evolution at fixed t . For example, evolution along the left vertical leg is described by the operator

$$U_{vl} = \mathcal{T}_x e^{-i \int_{-x_0}^{x_0} H_1(-t_0, x) dx},$$

where the corner points of the paths are taken as $t_0, x_0 \rightarrow \infty$, with the limit $t_0 \rightarrow \infty$ taken first.

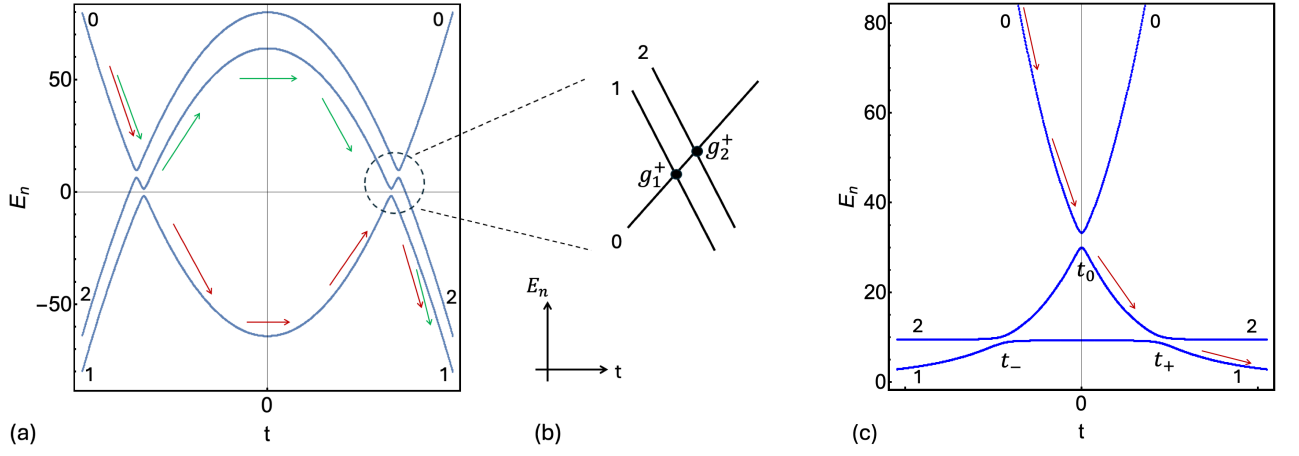


FIG. 4. (a) Eigenvalues of the Hamiltonian (26) as functions of $t = \sqrt{|x|}\tau$ at large negative x (blue curves). Here, $x = -16$; $\alpha_1 = \alpha_2 = 0.1$, $\varphi_1 = \pi/3$, $\varphi_2 = 3\pi/4$. The values of $u_1(x)$ and $u_2(x)$ are approximated by asymptotic formulas in Eq. (8). The Hamiltonian (26) is written in the basis of diabatic states. The labels 0, 1, 2 define the convention for the diabatic state indices. The diabatic states coincide asymptotically with the eigenstates as $t \rightarrow \pm\infty$. The red and green arrows show two semiclassical trajectories that originate on diabatic level 0 as $t \rightarrow -\infty$ and terminate at level 1 as $t \rightarrow +\infty$. The dashed circle encloses the behavior of the energy levels near the pseudo-time point $t = \sqrt{|x|}/2$. (b) Near $t = \sqrt{|x|}/2$, the dynamics is described by the exactly solvable DOM for three levels that cross linearly at fixed couplings g_1^+ and g_2^+ . The diagram of diabatic levels shows only the time dependence of diagonal elements of the Hamiltonian, which in the DOM are straight lines in the time-energy plot. (c) Eigenvalues of the Hamiltonian $H(t, x) + x^{3/2}(4\tau^2 + 1)\hat{1}$, as functions of $t = \sqrt{x}\tau$ at large positive x (blue). Here, $x = 10$, $A = 0.2$, $\rho = 0.12$, $e = 1.2$. A term proportional to $\hat{1}$ was added to the Hamiltonian to expose the spectrum better. The values of $u_1(x)$ and $u_2(x)$ are approximated by asymptotic formulas in Eqs. (9) and (10), respectively. The red arrows show the unique path that connects diabatic levels 0 and 1. At large positive x , it passes through two avoided crossing points near times t_0 and t_+ .

Let $|k\rangle$, where $k = 0, 1, 2$, be the diabatic states, in which basis the Hamiltonians H and H_1 are written in Eq. (4). For $t_0 \rightarrow \infty$, these states coincide with the eigenstates of $H_1(-t_0, x)$. The evolution along the left and right legs of P_∞ is adiabatic, resulting only in phase factors $e^{\pm 2it_0 x_0}$. Thus, only the horizontal segment of P_∞ contributes to the inter-state transition amplitudes.

Both the horizontal part of P_∞ and the path P , describe unitary quantum evolution over a pseudo-time $t \in (-t_0, t_0)$ at large positive and large negative x , respectively. Since the operator $H(t, x)$ depends on $u_{1,2}(x)$, the relations between the asymptotic values of $u_{1,2}(x)$ as $x \rightarrow \pm\infty$ are obtained by equating U_P to U_{P_∞} . Since the inter-state transition amplitudes are determined by the horizontal paths, at either large

positive or large negative x , both evolution operators can be evaluated using the WKB approach, which becomes exact in the limits $x \rightarrow \pm\infty$.

B. WKB analysis in the limit $x \rightarrow -\infty$

In this case, there are two resonant regions for $t \in (-t_0, t_0)$ near $t = \pm\sqrt{|x|}/2$, where all nonadiabatic transitions occur. For large $|x|$, these resonances are well separated. By rescaling time

$$t = \tau\sqrt{|x|}, \quad (25)$$

the Schrödinger equation (20) is transformed to $i\frac{d}{d\tau}|\Psi\rangle = H(\tau)|\Psi\rangle$, where

$$H(\tau) = \begin{bmatrix} |x|^{3/2}(4\tau^2 - 1) - 2\sqrt{|x|}(u_1^2(x) + u_2^2(x)) & -4|x|\tau u_1 - 2i\sqrt{|x|}u_1' & -4|x|\tau u_2 - 2i\sqrt{|x|}u_2' \\ -4|x|\tau u_1 + 2i\sqrt{|x|}u_1' & -|x|^{3/2}(4\tau^2 - 1) + 2\sqrt{|x|}u_1(x)^2 & 2\sqrt{|x|}u_1(x)u_2(x) \\ -4|x|\tau u_2 + 2i\sqrt{|x|}u_2' & 2\sqrt{|x|}u_1(x)u_2(x) & -|x|^{3/2}(4\tau^2 - 1) + 2\sqrt{|x|}(e + u_2(x)^2) \end{bmatrix}. \quad (26)$$

The time-dependent spectrum of this Hamiltonian for large negative x is shown in Fig. 4(a). Near $\tau = \pm 1/2$, additional simplifications follow. Let

$$g_{1,2}^- \equiv 2(|x|u_{1,2} - i\sqrt{|x|}u'_{1,2}).$$

After shifting the time variable to $\tau_m = \tau + 1/2$, the Hamilto-

nian in the vicinity of $\tau_m = 0$ reduces to the three-state DOM Hamiltonian with one level crossing linearly two parallel levels:

$$H_{-1/2}(\tau_m) = \begin{bmatrix} -4|x|^{3/2}\tau_m & g_1^- & g_2^- \\ (g_1^-)^* & 4|x|^{3/2}\tau_m & 0 \\ (g_2^-)^* & 0 & 4|x|^{3/2}\tau_m + 2\sqrt{|x|}e \end{bmatrix}.$$

Similarly, consider the time interval near $\tau = 1/2$ and keep only the relevant x -dependent terms. Introduce the couplings

$$g_{1,2}^+ = -2(|x|u_{1,2} + i\sqrt{|x|}u'_{1,2}).$$

After a shift of time as $\tau_p = \tau - 1/2$, the Hamiltonian near $\tau_p = 0$ is again the DOM:

$$H_{1/2}(\tau_p) = \begin{bmatrix} 4|x|^{3/2}\tau_p & g_1^+ & g_2^+ \\ (g_1^+)^* & -4|x|^{3/2}\tau_p & 0 \\ (g_2^+)^* & 0 & -4|x|^{3/2}\tau_p + 2\sqrt{|x|}e \end{bmatrix}.$$

The diabatic level diagram for $H_{1/2}$ is shown in Fig. 4(b). The two parallel levels may be close to one another, so that all three states interact simultaneously near the avoided crossings. Nevertheless, this model is solvable analytically.

The DOM exact solution for the scattering amplitudes coincides with the prediction of the independent crossing approximation, in which each encountered diabatic level crossing is treated as an independent two-state Landau-Zener transition between the crossing energy levels, followed by adiabatic evolution between successive level crossings [10]. Therefore, the entire calculation of the elements of the evolution matrix U_P reduces to identifying semiclassical trajectories connecting the initial and final states and then finding the corresponding quantum amplitudes using the independent crossing approximation. An example of two semiclassical trajectories connecting the initial state $|0\rangle$ to the final state $|1\rangle$ is shown by the red and green arrows in Fig. 4(a). The transition amplitudes between diabatic states are obtained using the scattering matrix for the Landau-Zener model (listed, e.g., in Chapter 5 of Ref. [10]) to describe transitions between pairs of states at any diabatic level intersection. Between such pairwise scatterings, the system undergoes adiabatic evolution with energies that can be estimated within second-order quantum perturbation theory in the small parameter $1/|x|$.

This WKB approach is equivalent to the textbook independent crossing approximation, which is widely used in theoretical physics and described, e.g., in Section 5.4 of [10]. This version of WKB was used in the derivation of transition amplitudes in multistate Landau-Zener models [28]. The advantage of this approach over the WKB analysis commonly used in studies of Painlevé equations [2] is that the pseudo-time t is never treated as a complex variable, so there is no need to analyze the full Stokes phenomenon to obtain the evolution matrix U_P .

In the present case, the full matrix U_P is not required. It is sufficient to assume that initially the system is in state $|0\rangle$, which has the highest energy as $t \rightarrow -\infty$, thus leading to the derivation of transition amplitudes $U_{P,00}$, $U_{P,10}$, and $U_{P,20}$.

C. WKB analysis as $x \rightarrow +\infty$

This limit is simpler because, as illustrated in Fig. 4(c), the level crossing pattern leads only to three elementary avoided crossings between pairs of levels. These crossings are well

separated both in energy and in time t . For example, the times of diabatic level crossings are given by $t_0 = 0$ and $t_{\pm} \approx \pm x/(4\sqrt{e})$. Therefore, each crossing is described by the scattering matrix for the two-state Landau-Zener model. Moreover, for the initial conditions with only level 0 populated, the avoided crossing at t_- is irrelevant, so only a single trajectory connects the initial state $|0\rangle$ to any final diabatic state. Therefore, path interference does not occur. Figure 4(c) illustrates this property by showing the only semiclassical trajectory connecting levels 0 and 1.

To calculate the scattering amplitudes using the asymptotically exact WKB, the functions $u_{1,2}(x)$ as $x \rightarrow +\infty$ were assumed to take the form given in Eqs. (9) and (10) with unknown parameters, including at logarithmic phase contributions. Near each avoided crossing, the couplings were expressed in terms of these unknown parameters, and the scattering amplitudes were estimated using the known scattering matrix for the Landau-Zener model.

After obtaining the amplitudes of $U_{P,k0}$, where $k = 0, 1, 2$, separately for P and P_{∞} , the WKB results were compared order by order in powers of x and t_0 , down to $O(1)$ contributions to the phase and amplitude. Terms that depended on t_0 and on high powers of x on both sides then canceled, leaving the connection formulas written in Eqs. (13)-(17) and fixing the logarithmic x -dependence in Eqs. (9) and (10).

V. EXCITATIONS AFTER UNSTABLE VACUUM DECAY

The system in Eqs. (6) and (7) was previously introduced in [32, 33], where it described a passage through a phase transition in scalar field theory. It can be interpreted as Hamiltonian dynamics, in which x is associated with physical time, t (not to be confused with the pseudo-time introduced in the previous section), and $u_1(t)$ and $u_2(t)$ are coordinates of a particle with two degrees of freedom. Let $\mathbf{X} = (u_1, u_2)$, and the corresponding time-dependent Hamiltonian is

$$\mathcal{H}(t) = \frac{\mathbf{P}^2}{2} - t\frac{\mathbf{X}^2}{2} + \frac{\mathbf{X}^4}{2} + \frac{eu_2^2}{2}, \quad (27)$$

where $\mathbf{P} = (P_1, P_2)$ is the vector of momenta canonically conjugated to u_1 and u_2 , and where $\mathbf{X}^2 \equiv u_1^2 + u_2^2$. The system in Eqs. (6) and (7) follows from Newton's equations of motion with the Hamiltonian (27).

In the limits $t \rightarrow \pm\infty$, the potential energy for this classical motion is that of a harmonic oscillator, so the amplitudes $\alpha_{1,2}$ are related to the asymptotically conserved, as $t \rightarrow -\infty$, adiabatic invariants [10, 12].

$$\mathcal{J}_{1,2} \equiv \frac{\alpha_{1,2}^2}{2}.$$

Similarly, I_1 and I_2 from Eq. (11) are identified as asymptotically conserved adiabatic invariants as $t \rightarrow +\infty$. Then, $\varphi_{1,2}$ and $\phi_{1,2}$ are the angles canonically conjugated to, respectively, $\mathcal{J}_{1,2}$ and $I_{1,2}$.

According to [32, 33], this classical dynamics appears as a saddle-point solution for a quantum field theory describing a time-dependent passage through a second-order quantum phase transition. The difference between $\mathcal{J}_{1,2}$ and $I_{1,2}$ captures inevitable nonadiabatic effects as the classical phase space trajectory passes through a separatrix. Physically, this event corresponds to crossing the critical point of a phase transition in the corresponding field theory [33]. Semiclassically, the actions are related to the numbers of produced quasiparticles: I_1/\hbar for the number of Higgs bosons and I_2/\hbar for the number of Goldstone bosons. The latter acquire a small mass due to the symmetry breaking term $\propto e$ in Eq. (27). The analysis in [32] did not provide explicit connection formulas but made several observations that can now be verified.

Thus, a useful feature of Eqs. (14) and (16) is that I_1 and I_2 depend on e only through the angles Φ_1 and Φ_2 , which themselves depend linearly on the initial phases φ_1 and φ_2 . Therefore, $\langle I_1 \rangle$ and $\langle I_2 \rangle$ are independent of e , where the brackets denote averaging over a uniform distribution of φ_1 and φ_2 . This invariance of the averaged actions was conjectured in [32] based on less rigorous analytical arguments and numerical simulations, and is now confirmed.

Next, the solution in Eqs. (13)-(17) exhibits asymmetry amplification, which was the main finding in [32]. No matter how small the symmetry breaking parameter e is, the dynamics for $u_1(t)$ and $u_2(t)$ strongly differ from one another as $t \rightarrow +\infty$. While $u_1(t)$ has a monotonically growing component, the asymptotic solution for $u_2(t)$ oscillates around zero. Note that if e changes sign, the asymptotic solutions in Eqs. (9) and (10) are obtained by switching indices 1 and 2. The solution at $e = 0$ reduces to the standard P-II solution, which is unstable in the present context.

The study in [32] also addressed the following question: Given that initially the system is nearly at the quantum vacuum state, which corresponds, in dimensionless variables here, to

$$\mathcal{J}_1 = \mathcal{J}_2 \equiv \mathcal{J} \ll 1, \quad (28)$$

what are the values of the adiabatic invariants as $t \rightarrow +\infty$? Averaging over the initial phases φ_1 and φ_2 was required.

Using that $\int_0^{2\pi} \ln(2|\sin(\Phi)|) d\Phi = 0$, averaging Eq. (17) over $\varphi_{1,2}$ at conditions in Eq. (28) gives that

$$\langle I_2 \rangle + 2\langle I_1 \rangle \approx \frac{1}{2\pi} \ln \left(\frac{1}{2\pi\mathcal{J}} \right). \quad (29)$$

Similarly, Eq. (14) with Eq. (28) lead to

$$\langle I_1 \rangle \approx \frac{1}{4\pi} \left[\ln \left(\frac{1}{2\pi\mathcal{J}} \right) - c_1 \right], \quad (30)$$

where

$$c_1 = \frac{1}{\pi^2} \iint_0^\pi \ln[4 - 2\cos(2\Phi_1) - 2\cos(2\Phi_2)] d\Phi_1 d\Phi_2 \approx 1.166. \quad (31)$$

Substituting Eqs. (30) and (31) into Eq. (29) leads also to

$$\langle I_2 \rangle \approx \frac{c_2}{2\pi}, \quad c_2 = c_1 \approx 1.166. \quad (32)$$

Expressions for $\langle I_1 \rangle$ and $\langle I_2 \rangle$ in Eqs. (30) and (32) were conjectured in [32] for $\mathcal{J} \ll 1$ without an analytical derivation of $c_{1,2}$, while numerical simulations in [32] estimated that $c_1 \approx 1.14$ and $c_2 \approx 1.19$, with an uncertainty in the last significant digit. This agrees well with the analytically derived values of these coefficients in Eq. (32). Curiously, the value of the double phase integral in Eq. (31), ≈ 1.166 , is the famous square-lattice spanning tree constant [34].

VI. CONCLUSION

When a system of nonlinear equations emerges from consistency conditions (3) for matrix operators, the nonlinear problem is effectively described by a linear one. The difficulty for higher-order systems of nonlinear equations often lies in the lack of a fully analytical solution of the associated linear model, even when WKB methods are applicable. Nevertheless, the class of known fully solvable multistate linear systems has been growing recently. Any of the newly solved linear systems may emerge in the WKB analysis enabled by the consistency conditions for a certain nonlinear system. The present article provides an example of such a situation, leading to analytical connection formulas for asymptotic solutions of two coupled P-II equations with a minimally broken symmetry.

Author thanks Prof. Alexander Its for useful discussions. This work was carried out under the auspices of the U.S. DoE through the Los Alamos National Laboratory, operated by Triad National Security, LLC (Contract No. 892333218NCA000001).

* nsinitsyn@lanl.gov

- [1] A. R. Its and A. A. Kapaev, *Mathematics of the USSR-Izvestiya* **31**, 193 (1988).
- [2] A. S. Fokas, A. R. Its, A. A. Kapaev, and V. Y. Novokshenov, *Painlevé Transcendents: The Riemann-Hilbert Approach*, Mathematical Surveys and Monographs (American Mathematical Society, 2006).
- [3] J. Baik, R. Buckingham, J. DiFranco, and A. Its, *Nonlinearity* **22**, 1021 (2009).
- [4] P. Kokocki, *Studies in Applied Mathematics* **144**, 504 (2020).
- [5] T. J. Bothner and R. Buckingham, *Communications in Mathematical Physics* **359**, 223 (2017).
- [6] A. P. Itin and P. Törmä, *Phys. Rev. A* **79**, 055602 (2009).
- [7] V. G. Sadhasivam, F. Suzuki, B. Yan, and N. A. Sinitsyn, *Nat. Commun.* **15**, 10246 (2024).
- [8] S.-Y. Lee, R. Teodorescu, and P. Wiegmann, *Physica D: Nonlinear Phenomena* **240**, 1080 (2011), arXiv:1005.0369 [nlin.SI].
- [9] S. Banerjee and N. A. Sinitsyn, *Phys. Rev. E* **108**, 034212 (2023).

- [10] N. A. Sinitsyn and V. L. Pokrovsky, *Quasi-Adiabatic Effects: Introduction to Geometric Phases and Landau-Zener Transitions*, Oxford Graduate Texts (Oxford University Press, Oxford, United Kingdom, 2026) hardcover (Feb. 5 2026).
- [11] A. R. Its, F. Mezzadri, and M. Y. Mo, *Communications in Mathematical Physics* **284**, 117 (2008).
- [12] L. M. Zelenyi, A. I. Neishtadt, A. V. Artemyev, D. L. Vainchtein, and H. V. Malova, *Physics–Uspekhi* **56**, 347 (2013).
- [13] A. Neishtadt, A. Artemyev, and D. Turaev, *Chaos* **29**, 051104 (2019).
- [14] M. G. Clerc, J. D. Dávila, M. Kowalczyk, P. Smyrnelis, and E. Vidal-Henriquez, *Calculus of Variations and Partial Differential Equations* **56**, 93 (2017).
- [15] T. Bothner and K. Liechty, *Nonlinearity* **26**, 1449 (2013).
- [16] N. A. Sinitsyn and V. Y. Chernyak, *J. Phys. A: Math. Theor.* **50**, 255203 (2017).
- [17] N. A. Sinitsyn and F. Li, *Phys. Rev. A* **93**, 063808 (2016).
- [18] N. A. Sinitsyn, E. Yuzbashyan, V. Y. Chernyak, A. Patra, and C. Sun, *Phys. Rev. Lett.* **120**, 190402 (2018).
- [19] V. Y. Chernyak, N. A. Sinitsyn, and C. Sun, *Phys. Rev. B* **100**, 224304 (2019).
- [20] J. Lin and N. A. Sinitsyn, *J. Phys. A: Math. Theor.* **47**, 175301 (2014).
- [21] F. Li, V. Y. Chernyak, and N. A. Sinitsyn, *Phys. Rev. Lett.* **121**, 190601 (2018).
- [22] B. Yan and N. A. Sinitsyn, *Nat. Commun.* **13**, 2212 (2022).
- [23] S. Barik, L. Bakker, V. Gritsev, J. Minář, and E. A. Yuzbashyan, arXiv preprint (2025), [arXiv:2507.10856](https://arxiv.org/abs/2507.10856).
- [24] P. R. Pasnoori and E. A. Yuzbashyan, Exact many-body wavefunction of the Kondo model with time-dependent interaction strength (2025), [arXiv:2509.05640 \[cond-mat.str-el\]](https://arxiv.org/abs/2509.05640).
- [25] P. R. Pasnoori, *Phys. Rev. B* **112**, L060409 (2025).
- [26] P. R. Pasnoori, *Phys. Rev. B* **113**, 094514 (2026).
- [27] Y. N. Demkov and V. I. Osherov, *Zh. Eksp. Teor. Fiz.* **53**, 1589 (1967), *sov. Phys. JETP* **26**, 916 (1968), English translation.
- [28] V. Y. Chernyak, N. A. Sinitsyn, and C. Sun, *J. Phys. A: Math. Theor.* **51**, 245201 (2018).
- [29] V. Y. Chernyak, F. Li, C. Sun, and N. A. Sinitsyn, *J. Phys. A: Math. Theor.* **53**, 295201 (2020).
- [30] L. D. Faddeev and L. A. Takhtajan, *Hamiltonian Methods in the Theory of Solitons* (Springer, New York, 1987).
- [31] L. D. Landau and E. M. Lifshitz, *Mechanics, Course of Theoretical Physics Vol. 1*, 3rd ed. (Pergamon, Oxford, 1980).
- [32] B. Tyagi, F. Suzuki, V. Y. Chernyak, and N. A. Sinitsyn, *Phys. Rev. A* **111**, 032205 (2025).
- [33] F. Suzuki, R. K. Malla, and N. A. Sinitsyn, *Phys. Rev. A* **112**, 013307 (2025).
- [34] G. M. Viswanathan, *Phys. Rev. E* **95**, 062138 (2017).